# General relativistic corrections to the weak lensing convergence power spectrum

John T. Giblin, Jr.,[1,2] James B. Mertens,[2] Glenn D. Starkman,[2] and Andrew R. Zentner[3]

[1]*Department of Physics, Kenyon College, 201 N College Rd, Gambier, Ohio 43022, USA*
[2]*CERCA/ISO, Department of Physics, Case Western Reserve University,*
*10900 Euclid Avenue, Cleveland, Ohio 44106, USA*
[3]*Department of Physics and Astronomy, University of Pittsburgh, 100 Allen Hall,*
*3941 O'Hara Street, Pittsburgh, Pennsylvania 15260, USA*
(Received 25 July 2017; published 20 November 2017)

We compute the weak lensing convergence power spectrum, $C_\ell^{\kappa\kappa}$, in a dust-filled universe using fully nonlinear general relativistic simulations. The spectrum is then compared to more standard, approximate calculations by computing the Bardeen (Newtonian) potentials in linearized gravity and partially utilizing the Born approximation. We find corrections to the angular power spectrum amplitude of order ten percent at very large angular scales, $\ell \sim 2$–$3$, and percent-level corrections at intermediate angular scales of $\ell \sim 20$–$30$.

## I. INTRODUCTION

Weak lensing calculations rely on a number of assumptions in order to improve tractability of models. These include physical assumptions, such as the Born approximation, where physical arguments are used to justify neglecting sub-dominant effects. Further assumptions are made when modeling the gravitational physics of lensed systems, in particular the assumption that a linearized gravitational model provides a sufficiently accurate description of the dynamics of the evolution of the Universe as well as the geodesic equations describing propagation of light. Here, we explore the impact of these assumptions on weak lensing convergence calculations by comparing standard, commonly used calculations to a fully general relativistic treatment of the problem. We find these approximations are accurate only to within a few percent on large angular scales. The relative magnitude of corrections is found to increase on larger angular scales, and lessen on smaller angular scales.

Such observations of weak lensing convergence power spectra are among the primary science goals of the ongoing Dark Energy Survey (DES) and Hyper Suprime-Cam (HSC) Subaru Strategic Survey, as well as the forthcoming surveys of the Large Synoptic Survey Telescope (LSST), the Euclid mission, and Wide-Field InfraRed Survey Telescope (WFIRST). The primary driver behind these measurements is their potential to use lensing power spectra to constrain cosmology, particularly the cause of cosmic acceleration [1] and neutrino mass (for example, Refs. [2–4]). Observationally viable models of dark energy and values of neutrino masses induce only subtle alterations to lensing power spectra on the order of a few percent. Consequently, it is of critical importance to produce theoretical predictions for lensing power spectra that are both very precise and very accurate so that the data are not misinterpreted (e.g., Refs. [3,5,6]). This continues to be one of the challenges to the exploitation of weak lensing observations for cosmological analyses.

Carefully examining the physical and perturbative approximations made in the context of lensing measurements requires a number of subtle considerations in order to compare to a fully relativistic treatment, ranging from the gauge-dependent nature of variables used in calculations to the particular way in which averaged quantities are utilized. We attempt to remain self-consistent in our treatment of this problem, and to explicitly define the quantities we consider and approximations we use. We begin by defining angular diameter distances and convergence in terms of optical scalars, and describe the $3 + 1$ framework we use to numerically integrate Einstein's equations. We then compute the Bardeen (Newtonian) gravitational potentials, use these potentials to obtain the weak lensing convergence field in an approximate setting, and compare the two models.

Past literature has explored the magnitude of corrections to observables due to commonly made assumptions [7,8], speculating that contributions from nonlinear gravitational effects can lead to approximately percent-level corrections, contingent upon the specific statistical measure being studied [9–12]. Here, we perform the first such study in a fully relativistic setting, utilizing simulations of a universe containing a cosmologically-motivated spectrum of density fluctuations in a perfect, pressureless "dust" fluid. We find percent-level corrections to the convergence power spectrum at $\ell \sim 10$–$20$. The relative importance of corrections is found to increase at smaller $\ell$, becoming of order ten percent at $\ell$ of a few. At higher $\ell$, the relative importance of relativistic corrections is found to decrease—although perhaps a physical effect, this may also be a consequence

of the spectrum of perturbations that we used, which contains only long-wavelength modes.

We begin by briefly detailing the methods we use to perform the fully relativistic calculation and the approximate calculations we compare to. We then present a quantitative comparison of simulated quantities using the two methods. We begin in Sec. II by describing the different formalisms we utilize to perform numerical calculations. In Sec. III we describe initial conditions for the toy universes we utilize, and in Sec. IV we detail results from numerical simulations.

## II. FORMALISM

### A. Raytracing in the BSSNOK formulation

The field of numerical relativity has evolved over the past several decades to become a standard numerical tool in contemporary physics. The field has progressed to the point where it can model physics ranging from systems of strongly gravitating compact objects in a fully relativistic, cosmological setting [13–15], to the dynamics of perfect fluids as they interact on cosmological length scales [16–18]. The BSSNOK formulation is a commonly used numerical scheme that has been demonstrated capable of modeling such systems with a high degree of accuracy, and importantly, numerical stability [19–21].

The BSSNOK system of equations is a $3 + 1$ conformal decomposition of the Einstein field equations. In this language, the line element is

$$ds^2 = -\alpha^2 dt^2 + e^{4\phi}\bar{\gamma}_{ij}(dx^i + \beta^i dt)(dx^j + \beta^j dt), \quad (1)$$

where $e^{4\phi}\bar{\gamma}_{ij}$ is the spatial metric, and $\bar{\gamma}_{ij}$ is a unit-determinant matrix. The parameters $\alpha$ and $\beta^i$ are respectively known as the lapse and shift. Einstein's field equations can be written in terms of these variables as a system of first-order dynamical equations,

$$\partial_t \phi = -\frac{1}{6}\alpha K + \beta^i \partial_i \phi + \frac{1}{6}\partial_i \beta^i \quad (2)$$

$$\partial_t \bar{\gamma}_{ij} = -2\alpha\bar{A}_{ij} + \beta^k \partial_k \bar{\gamma}_{ij} + \bar{\gamma}_{ik}\partial_j \beta^k + \bar{\gamma}_{kj}\partial_i \beta^k - \frac{2}{3}\bar{\gamma}_{ij}\partial_k \beta^k \quad (3)$$

$$\partial_t K = -\gamma^{ij}D_j D_i \alpha + \alpha\left(\bar{A}_{ij}\bar{A}^{ij} + \frac{1}{3}K^2\right) + 4\pi\alpha(\rho + S) + \beta^i \partial_i K \quad (4)$$

$$\partial_t \bar{A}_{ij} = e^{-4\phi}(-(D_i D_j \alpha) + \alpha(R_{ij} - 8\pi S_{ij}))^{TF} + \alpha(K\bar{A}_{ij} - 2\bar{A}_{il}\bar{A}^l_j) + \beta^k \partial_k \bar{A}_{ij} + \bar{A}_{ik}\partial_j \beta^k + \bar{A}_{kj}\partial_i \beta^k - \frac{2}{3}\bar{A}_{ij}\partial_k \beta^k. \quad (5)$$

The lapse and shift are considered gauge variables, and may be freely chosen. An additional auxiliary variable, a contraction of a conformal Christoffel symbol, $\bar{\Gamma}^i = \bar{\gamma}^{jk}\bar{\Gamma}^i_{jk}$, is evolved to improve numerical stability properties of the system according to

$$\partial_t \bar{\Gamma}^i = -2\bar{A}^{ij}\partial_j \alpha + 2\alpha(\bar{\Gamma}^i_{jk}\bar{A}^{jk} - \frac{2}{3}\bar{\gamma}^{ij}\partial_j K - 8\pi\bar{\gamma}^{ij}S_j + 6\bar{A}^{ij}\partial_j \phi) + \beta^j \partial_j \bar{\Gamma}^i - \bar{\Gamma}^j \partial_j \beta^i + \frac{2}{3}\bar{\Gamma}^i \partial_j \beta^j + \frac{1}{3}\bar{\gamma}^{li}\partial_l \partial_j \beta^j + \bar{\gamma}^{lj}\partial_l \partial_j \beta^i, \quad (6)$$

and is used when to computing the Ricci tensor and scalar.

Likewise, we can integrate the optical scalar equations [22] using the full framework of general relativity. Optical integration through a spacetime involves tracking beam "areas" along photon geodesics. The cosmological observable we compute here is the angular diameter distance, $D_A \equiv \ell/\Omega$, for an object with some physical length $\ell$ that subtends an angle $\Omega$ of an observer's sky. The optical scalar equations are valid in the limit of infinitesimal beams, or in the limit that both $\ell$ and $\Omega$ are small, although recent work may offer a way of working around this limitation [23]. The optical scalar equations assume photons do not interact, or that the beam follows photon geodesics and neither back-react nor interact with other matter in the universe. The optical scalar equations are given by

$$\frac{d^2}{d\lambda^2}\ell = \ell(\mathcal{R} - \sigma^2) \quad (7)$$

and

$$\frac{d}{d\lambda}(\ell^2 \sigma) = \ell^2 \mathcal{W}, \quad (8)$$

for some affine parameter $\lambda$ along a photon path, beam area $\ell$, shear rate $\sigma$, and Ricci and Weyl optical scalars, $\mathcal{R}$ and $\mathcal{W}$. Further details about these equations and our previous work numerically integrating these equations can be found in [24] and references therein.

As a final point of potential interest, we remark upon the computational complexity of the scheme described above. In synchronous gauge where $\alpha = 1$, used in this work, and indeed in the vast majority of gauges typically used in numerical relativity, Einstein's equations are completely local, so calculations are $\mathcal{O}(N)$ for some number $N$ of discretized elements of interest (grid points, particles, ...). This is in contrast to the use of a nonlocal gauge, where calculations typically scale as $\mathcal{O}(N \log N)$. This penalty is incurred when using Newtonian gauge, commonplace in N-body simulations, and is encountered in this work when we compute the Bardeen potentials. The drawbacks of a fully relativistic calculation are due in part to the increased number of algebraic calculations involved, but perhaps

more important is the need to resolve luminal propagation. However, these penalties should also be incurred by any code wishing to reliably integrate geodesics, resolve luminally propagating phenomena, or resolve higher-order gravitational effects, even within a framework of linearized gravity.

## B. Computing convergence

Convergence in weak lensing may be defined in terms of angular diameter distances as

$$\kappa = \frac{\bar{D}_A - D_A}{\bar{D}_A},\tag{9}$$

where $\bar{D}_A$ is the angular diameter distance as defined in a pure-FLRW universe [25]. Defined this way, convergence is meaningful in a fully relativistic setting, i.e., no perturbative assumptions need to be made, and the above expression reduces to expressions found in cosmological literature in a Newtonian setting.

In a general relativistic setting, computing angular diameter distances, and thus convergence as defined in Eq. (9), requires integration of the optical scalar equations as detailed in Sec. II A. In Newtonian gauge (sometimes referred to as Poisson gauge or longitudinal gauge; here we follow the conventions of [26]), this task is simplified after making several assumptions, both perturbative and physical [11,12,27]. Typically, perturbative assumptions enter by modeling spacetime and matter dynamics within a linearized gravity framework, while the physical assumptions include assuming the behavior of the spacetime is sufficiently well-described by scalar degrees of freedom and perfect fluid components. Under these assumptions, this expression for weak lensing convergence can be written in terms of the Bardeen (Newtonian) potential $\Phi$,

$$\kappa = \int (r_s - r) \frac{r}{r_s} \nabla_\perp^2 \Phi dr,\tag{10}$$

where $r$ is the coordinate distance (in Newtonian gauge) along the path of integration (a line-of-sight), and $r_s$ is the total coordinate distance to an emitting source of interest. The gradient in this expression is transverse to the direction of propagation, $\hat{n}$, thus can alternatively be written in terms of a full Laplacian minus a component along this direction,

$$\nabla_\perp^2 \Phi = \nabla^2 \Phi - \partial_{\hat{n}}^2 \Phi.\tag{11}$$

The full Laplacian may be evaluated using the Hamiltonian constraint equation in Newtonian gauge linearized around an FLRW background in the presence of a perfect fluid, or Poisson's equation for gravity,

$$\nabla^2 \Phi = 4\pi a^2 \delta\rho + 12\pi a^2 (\bar{\rho} + \bar{p})\delta u.\tag{12}$$

We will also compute the radial coordinate using a radial-redshift relationship commonly enforced in the Born approximation,

$$r(z) = \int_0^z \frac{1}{H(z')} dz'.\tag{13}$$

This is the only time we use the Born approximation—the Bardeen potential and stress-energy quantities are evaluated along a true geodesic, computed using fully general relativistic expressions. Thus, both our exact and approximate calculations include effects related to deflections of photon trajectories, for example as studied in the context of lensing of the cosmic microwave background in [28,29], where such effects were found to be potentially detectable by future observations. The derivative of the Bardeen potential along the path of integration is also computed along this geodesic, with photon redshift rescaled to a coordinate expression using the above radial-redshift approximation. The second derivative is then computed with respect to this radial coordinate.

Often, the radial derivative and peculiar velocity contributions are neglected entirely; we do not include these assumptions in our analysis. However, in line with weak lensing literature, we have also neglected some first-order contributions to the relativistic expression for convergence (for example, gravitational redshift and ISW terms as described in [7]). The peculiar velocity contribution can be accounted for by adding a term proportional to the fluid velocity components at the source and observer, $\vec{v}_s$ and $\vec{v}_o$ along the line of sight $\hat{n}$ in Newtonian gauge [30], $\kappa \to \kappa + \kappa_v$, where

$$\kappa_v = -\frac{a}{\dot{a} \int dz/H}(\vec{v}_s - \vec{v}_o) \cdot \hat{n} + \vec{v}_s \cdot \hat{n}.\tag{14}$$

The final approximate expression for convergence we seek to integrate is thus

$$\kappa = \int (r_s - r) \frac{r}{r_s}(4\pi a^2 \delta\rho + 12\pi a^2(\bar{\rho} + \bar{p})\delta u - \partial_{\hat{n}}^2 \Phi)dr + \kappa_v.\tag{15}$$

For a final comparison, we compute this approximate expression, Eq. (15), and compare to Eq. (9), a fully general relativistic result.

As a final note, the precise magnitude of corrections will depend upon the background cosmological parameters that are chosen. To this end, we note that we compute $H(z)$, $a(z)$, and $\bar{D}_A(z)$ along geodesics using a background cosmology corresponding to the standard FLRW solution for a matter-dominated universe coincident with the choice used to set the initial conditions of our simulations. However, when computing the scale factor on a given spatial slice in order to compute Bardeen potentials, we

compute $a(t)$ using the conformally-averaged conformal factor on a spatial hypersurface and assuming a matter-dominated universe to determine $H(t)$. These choices do not significantly affect our results; the differences between backgrounds given by averaged values and FLRW values differ by less than a part in $10^6$ (i.e., backreaction is negligible).

## C. Computing Bardeen potentials from a fully relativistic simulation

The Bardeen potentials, or Newtonian potentials $\Phi$ and $\Psi$, may be computed from a known metric in an arbitrary gauge—here, we compute them using the synchronous gauge (geodesic slicing) metric. We obtain the Bardeen potentials by first performing a scalar-vector-tensor (SVT) decomposition of the metric linearized around a homogeneous FLRW background. We perform this

decomposition following Weinberg [26], writing the metric as a background plus perturbation,

$$g_{\mu\nu} = \bar{g}_{\mu\nu} + h_{\mu\nu}. \tag{16}$$

An ambiguity exists in this definition in that the choice of $\bar{g}_{\mu\nu}$ is arbitrary—any background metric will suffice—however the FLRW metric is chosen in a cosmological setting as we expect the dynamics of the spacetime to be well-described by such a background, so $\bar{g}_{\mu\nu} = \text{diag}(-1, a^2\delta_{ij})$. Fluctuations around this background are taken to be small so that quantities derived from $h_{\mu\nu}$ may be raised and lowered using purely the background metric with terms second-order in $h_{\mu\nu}$ dropped. The perturbed metric is then decomposed as

$$h_{\mu\nu} = \begin{pmatrix} h_{00} & h_{i0} \\ h_{0j} & h_{ij} \end{pmatrix} = \begin{pmatrix} -E & a(\partial_i F + G_i) \\ a(\partial_j F + G_j) & a^2(A\delta_{ij} + \partial_i\partial_j B + \partial_i C_j + \partial_j C_i + D_{ij}) \end{pmatrix}. \tag{17}$$

The vector and scalar functions are transverse with respect to the background metric,

$$\partial_i C^i = \partial_i G^i = \partial_i D^{ij} = 0, \tag{18}$$

and the tensor perturbation is trace-free, $D_i^i = 0$. Given that the $3 + 1$ metric in synchronous gauge is written as

$$g_{\mu\nu} = \begin{pmatrix} -1 & 0 \\ 0 & \gamma_{ij} \end{pmatrix}, \tag{19}$$

we immediately see that in synchronous gauge, a number of potentials are zero, $F = G_i = E = 0$. We can also see that the metric perturbations and their time derivatives (which will be needed to compute the Bardeen potentials) can be written in terms of BSSNOK variables as

$$h_{ij} = \gamma_{ij} - a^2\delta_{ij} \tag{20}$$

$$\dot{h}_{ij} = -2K_{ij} - 2a\dot{a}\delta_{ij} \tag{21}$$

$$\ddot{h}_{ij} = -2(\dot{K}_{ij} + (\dot{a}^2 + a\ddot{a})\delta_{ij}), \tag{22}$$

where $K_{ij} = e^{4\phi}\bar{A}_{ij} + \frac{1}{3}\bar{\gamma}_{ij}K$ is the extrinsic curvature, and its time derivative can be written in terms of BSSNOK variables,

$$\dot{K}_{ij} = 4\dot{\phi}e^{4\phi}\left(\bar{A}_{ij} + \frac{1}{3}\bar{\gamma}_{ij}K\right)$$
$$+ e^{4\phi}\left(\dot{\bar{A}}_{ij} + \frac{1}{3}\dot{\bar{\gamma}}_{ij}K + \frac{1}{3}\bar{\gamma}_{ij}\dot{K}\right). \tag{23}$$

From this, we can reconstruct the SVT scalar field A,

$$A = \frac{1}{2a^2}\left(h_{ii} - \frac{1}{\nabla^2}\partial_i\partial_j h_{ij}\right), \tag{24}$$

and B,

$$B = \frac{1}{\nabla^2}\left(\frac{h_{ii}}{a^2} - 3A\right), \tag{25}$$

with time-derivatives of $B$ being computed using time derivatives of $h_{ij}$. An ambiguity in this definition of $B$ allows for the addition of an arbitrary time-dependent function. To address this, we note that we specify the zero-mode of the inverse Laplacian to be zero. We numerically solve these equations for $A$ and $B$ in Fourier space. The remaining vector and tensor potentials may also be determined if desired, however we do not do so here. At this point, we have enough information to construct the Bardeen potentials. In terms of the synchronous gauge scalar potentials, these are given by

$$\Phi = -\frac{a}{2}(2\dot{a}\dot{B} + a\ddot{B})$$
$$\Psi = \frac{1}{2}(a\dot{a}\dot{B} - A). \tag{26}$$

Note that Weinberg's definitions $\Phi$ and $\Psi$ are opposite the more common convention.

As mentioned before, there is one further minor ambiguity: the scale factor $a$ can be chosen in several different ways. For example, it can be chosen to correspond to the average conformal factor $\langle e^{2\phi} \rangle$ in a particular slicing, or the FLRW solution corresponding to this value computed on the initial or final slices. For this work, we opt to choose a scale factor that coincides with the scale factor on the initial surface, and that evolves according to the standard matter-dominated Friedmann equations.

Converting density fluctuation amplitudes from synchronous gauge to Newtonian should be performed as well,

$$\delta\rho^N = \delta\rho^S + \frac{a^2}{2}\dot{B}\,\dot{\bar{\rho}}, \tag{27}$$

along with fluid 3-velocity velocity, $\delta u_i = \partial_i \delta u$,

$$\delta u^N = \delta u^S - \frac{a^2}{2}\dot{B}. \tag{28}$$

As a final note, although the synchronous gauge metric is not uniquely determined in terms of the Bardeen potentials, we do not transform variables from Newtonian to synchronous, and thus do not encounter this issue.

## III. INITIAL CONDITIONS

We set initial conditions by generating a random realization of a cosmologically-motivated power spectrum, similar to past work [31]. As the initial conditions we use are intended to mimic an inhomogeneous cosmology, we attempt to, at least approximately, match large-scale matter density fluctuations. At large scales, the power spectrum of density fluctuations is expected to scale as $P_\delta \propto k^1$, and at small scales as $P_\delta \propto k^{-3}$. We choose a spectrum that corresponds to these scalings,

$$P_{\delta\delta} = \frac{4}{3} P_* \frac{k/k_*}{1 + (k/k_*)^4/3} \times C(k, k_c), \tag{29}$$

with $k_*$ the peak frequency and $P_*$ the amplitude of the power spectrum. The function $C$ is included in order to introduce a short-wavelength cutoff scale, $k_c$, to exclude small-scale modes that are not well-resolved and can therefore lead to numerical instability or inaccuracy. In practice, this means resolving all modes by $\mathcal{O}(5-10)$ grid points or more on the initial surface. We choose $C$ to be a logistic function,

$$C(k, k_c) = \frac{1}{1 + e^{10(k-k_c)}}. \tag{30}$$

We additionally choose the initial peak frequency to correspond to a length scale of roughly 300 Mpc, and a

power spectrum amplitude that corresponds to a realistic RMS amplitude of the density. Although 8 Mpc scales are not well-resolved, we still use a power spectrum amplitude that corresponds to a $\sigma_8$ value (RMS density fluctuation amplitude smoothed on 8 Mpc scales) of $\sigma_8 \sim 0.8$. We simulate half of a Hubble volume and include modes down to $k^{-1} = 1/40 \ H^{-1} \sim 100$ Mpc. Smoothed on this scale, the expected RMS density amplitude is $\sigma_{100} \sim 0.07$ at the time of observation [32]. We choose our power spectrum amplitude such that the amplitude of the conformal RMS density fluctuations, defined as

$$\sigma_\rho = \sqrt{\frac{\int dV \sqrt{\gamma}(\bar{\rho}-\rho)^2}{\int dV \sqrt{\gamma}}}, \tag{31}$$

with the average density defined as

$$\bar{\rho} = \frac{\int dV \sqrt{\gamma}\rho}{\int dV \sqrt{\gamma}}, \tag{32}$$

approximately coincides with this value of $\sigma_{100}$.

The metric and matter fields on the initial surface must satisfy the Hamiltonian and momentum constraint equations. In terms of BSSN variables, these are given by

$$\mathcal{H} = 0 = \bar{\gamma}^{ij}\bar{D}_i\bar{D}_j e^\phi - \frac{e^\phi}{8}\bar{R} + \frac{e^{5\phi}}{8}\bar{A}^{ij}\bar{A}_{ij}$$
$$- \frac{e^{5\phi}}{12}K^2 + 2\pi e^{5\phi}\rho \tag{33}$$

and

$$\mathcal{M}^i = 0 = \bar{D}_j(e^{5\phi}\bar{A}^{ij}) - \frac{2}{3}e^{6\phi}\bar{D}^i K - 8\pi e^{10\phi}S^i. \tag{34}$$

We choose $\bar{A}_{ij} = 0$, and $\bar{\gamma}_{ij} = \delta_{ij}$, imposing the restriction that the 3-metric be conformally flat on the initial slice. The momentum constraint can be trivially solved by choosing the extrinsic curvature $K$ to be constant and the momentum variable $S^i$ to be zero, consistent with a fluid initially at rest. The Hamiltonian constraint equation can be solved by specifying the remaining metric components, and solving for the corresponding density. For the conformally flat metric we have chosen, the conformal Ricci scalar is zero, $\bar{R} = 0$. The remaining metric term in the Hamiltonian constraint is the $\nabla^2 e^\phi$ term, fluctuations of which will correspond to fluctuations in $\rho$. In order to produce density fluctuations described by the above cosmologically-motivated power spectrum, we choose the conformal factor $\phi$ to be described by a related power spectrum,

$$P_{\phi\phi} = k^{-4}P_{\delta\delta}. \tag{35}$$

We generate a Gaussian random realization of $\phi$ according to this prescription. The remaining metric variable $K$, the local expansion rate, is chosen to correspond to a desired

Hubble expansion rate. The density is then fixed by the Hamiltonian constraint equation. Further details on this method can be found in [31].

Although the initial conditions we use are qualitatively similar to those found in a cosmological setting, the setup we use does not precisely correspond to physical expectations. We therefore recognize this as a toy model, rather than a precision calculation. Nevertheless, we are hopeful that the effects we see here can provide a reliable indication of the order of magnitude of corrections to Newtonian calculations due to general relativistic effects, and that they can provide a qualitative indication of the relevance of relativistic effects to observations. Generalizing these initial conditions to more closely correspond to expectations from Newtonian or linear theory, but in a relativistic setting, will be an important future task.

The final ingredient required in order to specify the sky seen by an observer is, of course, an observer. In this work, we lay down initial conditions and integrate the simulation forward to a desired time of observation. We then place an observer at the center of our simulation volume and integrate along geodesics away from this observer in HEALPIX [33] directions, from the observer's spacetime point "backwards" in time. This observer, along with sources, are taken to be at rest in geodesic slicing, or to be comoving with the local fluid.

## IV. RESULTS

Here we present results from a simulation in which photon geodesics are integrated from an observer back in time to a redshift of $z = 0.25$. In particular, we compare Eq. (9) to Eq. (10). In order to compute the former of these we utilize the above $3 + 1$ formulation of Einstein's equations, thus integrating through a fully general relativistic spacetime including no approximations or reductions to the Einstein field equations. The latter of these expressions originates from a linearized, scalar gravity treatment, for which we additionally utilize the Born approximation in order to obtain a radial coordinate as described in Sec. II B.

In order to compute the angular power spectrum, we decompose the convergence field on the sky into spherical harmonics. The convergence field is written as

$$\kappa(\theta, \phi) = \sum_{lm} a_{lm} Y_{lm}(\theta, \phi). \tag{36}$$

From this, the angular power spectrum is then defined,

$$C_l^{\kappa\kappa} = \frac{1}{2l+1} \sum |a_{lm}^2|. \tag{37}$$

In practice, we compute the angular power spectrum by integrating angular diameter distances—and therefore convergences—in HEALPIX directions for an observer in our simulated universe. We then use standard HEALPIX routines
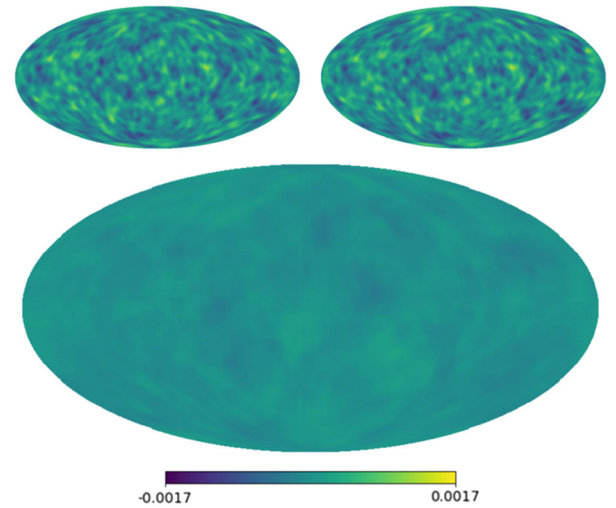


FIG. 1. Observed skies: top left is a sky generated using approximate theory [Eq. (10)], top right a relativistic sky [Eq. (9)], and bottom the difference between the two. These skies are generated using a HEALPIX resolution of Nside = 32, and all maps have had the angular monopole and dipole contributions removed.

to compute the power spectrum from the convergence maps we produce. Convergence maps are plotted in Fig. 1, depicting the difference between relativistic simulation results and approximate results. The power spectra that correspond to these images are shown in Fig. 2.

In order to obtain meaningful results, we must also compute the numerical error for convergence values along each geodesic. We do so by performing runs using a set of four resolutions in our simulation, $N^3 = 128^3$, $160^3$, $192^3$,
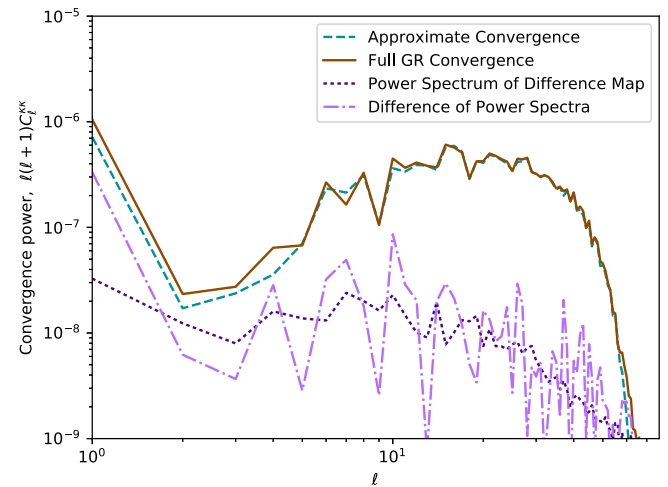


FIG. 2. Power spectra of the simulated skies shown in Fig. 1. The brown (solid) curve depicts results from a fully relativistic run, teal (dashed) from approximate theory, dark purple (dotted) the average power spectrum of the difference map, and light purple (dot-dashed) a direct subtraction of the GR and approximate power spectra.

and $256^3$. We Richardson extrapolate convergence values in the continuum limit by using different pairs of runs and assuming accumulated error is $\mathcal{O}(\Delta x)$ [24]. We then use the distribution of extrapolated values to provide us with a measure of uncertainty in these convergence values. The extrapolated values typically agree at one part in $10^4$, or at a level significantly smaller than the difference between convergences computed using approximate and relativistic methods. The uncertainty in extrapolated power spectra is also found to be accurate at this level. As an additional note, we compute power spectra using $\ell_{\max} \sim 2.4 \max(\ell)$ in HEALPIX in order to obtain more accurate results. The resulting numerical error in the spectra we present in this paper is then expected to be better than a part in $10^4$.

There is, in addition, sampling error—or cosmic variance—resulting from the limited number of simulations we run. In order to address this, we simulate twenty skies in total, and average the power spectra together. The resulting spectra are shown in Fig. 3, in which we find an $\ell$-dependent increase in the amplitude of the approximate power spectrum compared to the fully relativistic spectrum. Some remaining cosmic variance can be seen as ripples or wiggles in the power spectra; such effects may be expected to diminish as an increasing number of simulations are averaged over.

Finally, we remark on the potential origins of the discrepancies we see: are these due to nonlinear physics, the radial-redshift approximation, or merely artifacts of the gauge transformations we have performed? The amplitude of the Newtonian potentials, and amplitude of the components of the gauge transformation, are not large, being of

order a part in $10^5$ on these large scales. Fluctuations in the synchronous gauge metric itself, $\sigma_\phi/\phi$, are closer to a part in $10^4$, and second-order contributions to the convergence from shear terms in the optical scalar equations are also present at this level. One may therefore expect ambiguities due to gauge and nonlinear effects to be smaller than the observed percent-level corrections, indicating the remaining physical approximations may be breaking down.

The main physical approximation we utilize enters when computing the radial coordinate, Eq. (13), where we find that the perturbed and FLRW redshifts agree to roughly a part in $10^3$. The remaining discrepancy can ostensibly be explained by the physical approximations made in order to obtain Eq. (10) from the optical scalar equations [7]. However, as a final note, we also find that the Newtonian potentials $\Phi$ and $\Psi$ evolve towards percent-level disagreement, or that a significant gravitational slip develops, suggesting the system may also be evolving away from the linearized constraint equations typically enforced in a cosmological setting. Further exploration will be required to precisely characterize the physics at play here, and to determine how both physical and perturbative approximations are breaking down.

## V. DISCUSSION

In this manuscript, we have described the possibility of percent-level corrections to lensing power spectrum predictions due to a fully relativistic treatment of gravitational lensing by large-scale structure. This suggests circumspection in the utilization of weak lensing measurements to constrain cosmological parameters. However, a direct comparison of our work to prior literature on lensing cosmology is not possible at the present time. Due to computational limitations, we work within a toy, inhomogeneous Einstein-de Sitter cosmology, explore only large angular scales ($\ell \sim 10$), and only consider lensing out to a redshift of $z \sim 0.25$. By way of contrast, lensing by ongoing and forthcoming observational facilities is dominated by structure at significantly higher redshifts ($z \sim 0.6$–1), and the majority of the cosmological information is contained in lensing correlations on considerably smaller scales (significantly less than a degree, multipoles of $\ell \gtrsim 300$).

We also do not currently have a reliable method of extrapolating our results to the more practical case of small-scale lensing correlations induced by high-redshift, large-scale structure in a dark energy-dominated universe. However, it is interesting to speculate on the possible importance of our work in this context. Using the methods of [6,3] it is straightforward to estimate the potential impact of the systematic errors that we explore on the program to constrain cosmology using weak gravitational lensing correlations. For an LSST- or Euclid-like survey, we estimate that a one-percent systematic offset in the lensing power spectrum corresponds to a systematic error on the
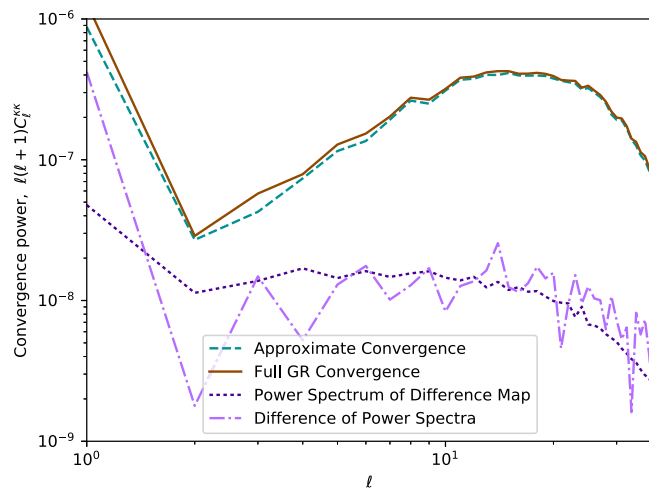


FIG. 3. Shown are averages of 20 power spectra obtained from independent simulations. The brown (solid) curve shows the fully relativistic power spectrum, and teal (dashed) the approximate spectrum. The dark purple (dotted) curve is the average power spectrum of the difference maps, and the light purple (dot-dashed) power spectrum the average of a direct subtraction of the GR and approximate power spectra.

inferred dark energy equation of state parameter, $w$, that is roughly twice the statistical error with which this parameter may be measured. We estimate a similar level of error for the neutrino mass. We argue that this is strong motivation to pursue fully relativistic lensing studies further. However, we emphasize that these estimates remain speculative as we do not yet understand the cosmology dependence, scale dependence, or redshift dependence of the effects we describe, and all of those factors can significantly alter these estimates.

Future studies may also wish to examine the behavior of specific dark energy or dark matter models in a fully relativistic context. Important effects have been considered using approximate treatments in the past, including baryonic physics [34], radiation [35], interactions of propagating light with contents of the Universe [36], and a more complete picture of phase space dynamics [37]. Incorporating such phenomenology into a fully general relativistic simulation has not yet been performed in a cosmological setting, and will be an important task for relativistic simulations in the coming years.

[1] D. H. Weinberg, M. J. Mortonson, D. J. Eisenstein, C. Hirata, A. G. Riess, and E. Rozo, Observational probes of cosmic acceleration, Phys. Rep. **530,** 87 (2013).

[2] J. Hamann, S. Hannestad, and Y. Y. Y. Wong, Measuring neutrino masses with a future galaxy survey, J. Cosmol. Astropart. Phys. 11 (2012) 052.

[3] A. Natarajan, A. R. Zentner, N. Battaglia, and H. Trac, Systematic errors in the measurement of neutrino masses due to baryonic feedback processes: Prospects for stage IV lensing surveys, Phys. Rev. D **90,** 063516 (2014).

[4] Y. Takeuchi and K. Kadota, Probing neutrinos from Planck and forthcoming galaxy redshift surveys, J. Cosmol. Astropart. Phys. 01 (2014) 046.

[5] D. Huterer and M. Takada, Calibrating the nonlinear matter power spectrum: Requirements for future weak lensing surveys, Astropart. Phys. **23,** 369 (2005).

[6] A. P. Hearin, A. R. Zentner, and Z. Ma, General requirements on matter power spectrum predictions for cosmology with weak lensing tomography, J. Cosmol. Astropart. Phys. 04 (2012) 034.

[7] L. Hui and P. B. Greene, Correlated fluctuations in luminosity distance and the (surprising) importance of peculiar motion in supernova surveys, Phys. Rev. D **73,** 123526 (2006).

[8] E. Di Dio and R. Durrer, Vector and tensor contributions to the luminosity distance, Phys. Rev. D **86,** 023510 (2012).

[9] K. Bolejko, C. Clarkson, R. Maartens, D. Bacon, N. Meures, and E. Beynon, Antilensing: The Bright Side of Voids, Phys. Rev. Lett. **110,** 021302 (2013).

[10] O. Umeh, C. Clarkson, and R. Maartens, Nonlinear relativistic corrections to cosmological distances, redshift and gravitational lensing magnification: I. Key results, Classical Quantum Gravity **31,** 202001 (2014).

[11] S. Andrianomena, C. Clarkson, P. Patel, O. Umeh, and J.-P. Uzan, Non-linear relativistic contributions to the cosmological weak-lensing convergence, J. Cosmol. Astropart. Phys. 06 (2014) 023.

[12] A. Petri, Z. Haiman, and M. May, Validity of the Born approximation for beyond Gaussian weak lensing observables, Phys. Rev. D **95,** 123503 (2017).

[13] E. Bentivegna and M. Korzynski, Evolution of a family of expanding cubic black-hole lattices in numerical relativity, Classical Quantum Gravity **30,** 235008 (2013).

[14] C.-M. Yoo and H. Okawa, Black hole universe with a cosmological constant, Phys. Rev. D **89,** 123502 (2014).

[15] E. Bentivegna, M. Korzyński, I. Hinder, and D. Gerlicher, Light propagation through black-hole lattices, J. Cosmol. Astropart. Phys. 03 (2017) 014.

[16] J. T. Giblin, J. B. Mertens, and G. D. Starkman, Departures from the Friedmann-Lemaitre-Robertston-Walker Cosmological Model in an Inhomogeneous Universe: A Numerical Examination, Phys. Rev. Lett. **116,** 251301 (2016).

[17] E. Bentivegna and M. Bruni, Effects of Nonlinear Inhomogeneity on the Cosmic Expansion with Numerical Relativity, Phys. Rev. Lett. **116,** 251302 (2016).

[18] J. T. Giblin, J. B. Mertens, and G. D. Starkman, A cosmologically motivated reference formulation of numerical relativity, Classical Quantum Gravity **34,** 214001 (2017).

[19] T. Nakamura, K. Oohara, and Y. Kojima, General relativistic collapse to black holes and gravitational waves from black holes, Prog. Theor. Phys. Suppl. **90,** 1 (1987).

[20] M. Shibata and T. Nakamura, Evolution of three-dimensional gravitational waves: Harmonic slicing case, Phys. Rev. D **52**, 5428 (1995).

[21] T. W. Baumgarte and S. L. Shapiro, On the numerical integration of Einstein's field equations, Phys. Rev. D **59**, 024007 (1998).

[22] R. K. Sachs, Gravitational waves in general relativity. 6. The outgoing radiation condition, Proc. R. Soc. Edinburgh, Sect. A **264**, 309 (1961).

[23] P. Fleury, J. Larena, and J.-P. Uzan, Weak gravitational lensing of finite beams, arXiv:1706.09383.

[24] J. T. Giblin, J. B. Mertens, and G. D. Starkman, Observable deviations from homogeneity in an inhomogeneous universe, Astrophys. J. **833**, 247 (2016).

[25] P. Fleury, J. Larena, and J.-P. Uzan, The theory of stochastic cosmological lensing, J. Cosmol. Astropart. Phys. 11 (2015) 022.

[26] S. Weinberg, Cosmology. (Oxford University Press, Oxford, 2008) https://global.oup.com/academic/product/9780198526827.

[27] A. Barreira, C. Llinares, S. Bose, and B. Li, RAY-RAMSES: A code for ray tracing on the fly in N-body simulations, J. Cosmol. Astropart. Phys. 05 (**2016**) 001.

[28] G. Marozzi, G. Fanizza, E. Di Dio, and R. Durrer, CMB-lensing beyond the Born approximation, J. Cosmol. Astropart. Phys. 09 (2016) 028.

[29] G. Fabbian, M. Calabrese, and C. Carbone, CMB weak-lensing beyond the Born approximation: A numerical approach, arXiv:1702.03317.

[30] N. Kaiser and M. J. Hudson, On the perturbation of the luminosity distance by peculiar motions, Mon. Not. R. Astron. Soc. **450**, 883 (2015).

[31] J. B. Mertens, J. T. Giblin, and G. D. Starkman, Integration of inhomogeneous cosmological spacetimes in the BSSN formalism, Phys. Rev. D **93**, 124059 (2016).

[32] D. H. Lyth and A. R. Liddle, *The primordial density perturbation: Cosmology, inflation and the origin of structure.* (Cambridge University Press, Cambridge, 2009) https://www.cambridge.org/9780521828499.

[33] K. M. Gorski, E. Hivon, A. J. Banday, B. D. Wandelt, F. K. Hansen, M. Reinecke, and M. Bartelman, HEALPix—A Framework for high resolution discretization, and fast analysis of data distributed on the sphere, Astrophys. J. **622**, 759 (2005).

[34] K. Osato, M. Shirasaki, and N. Yoshida, Impact of baryonic processes on weak-lensing cosmology: Power spectrum, nonlocal statistics, and parameter bias, Astrophys. J. **806**, 186 (2015).

[35] J. Adamek, J. Brandbyge, C. Fidler, S. Hannestad, C. Rampf, and T. Tram, The effect of early radiation in N-body simulations of cosmic structure formation, Mon. Not. R. Astron. Soc. **470**, 303 (2017).

[36] V. A. A. Sanghai, P. Fleury, and T. Clifton, Ray tracing and Hubble diagrams in post-Newtonian cosmology, J. Cosmol. Astropart. Phys. 07 (2017) 028.

[37] J. Adamek, D. Daverio, R. Durrer, and M. Kunz, General relativity and cosmic structure formation, Nat. Phys. **12**, 346 (2016).